Online ISSN: 2981-0396 Print ISSN: 2981-0388

International Journal of Iron & Steel Society of Iran

Journal Homepage: https://journal.issiran.com/

Research Article

Investigation of Mushy Zone Formation and Its Characteristics During Continuous Casting of Steel Billets with A Simple Modeling and Simulation Process

M. Alizadeh *[1]

Department of Materials Science and Engineering, School of Engineering, Meybod University, Meybod, Yazd, Iran

ARTICLE INFO

Keywords:

Continuous casting, Billet, Mushy zone, Medium carbon steel.

Article history:

Received 18 December 2024
Received in revised form 05 March 2025
Accepted 05 October 2025

ABSTRACT

In this research, simple modeling and simulation were used, and the dimensions and characteristics of the mushy zone in medium carbon steel during continuous casting were investigated. For this purpose, a numerical solution of the heat transfer equation as well as analytical microsegregation equations were used, and the following items were determined as mushy zone characteristics: mushy zone width, mushy core, mushy zone area, overall and local solidification time, local cooling rate, and brittle region characteristics. The width of the mushy zone increases up to a certain point along the length of the billet and then decreases to zero. The length of the billet over which the width of the mushy zone decreases from a maximum value to zero is called the mushy core in which the temperature gradient increases at an increasing rate. As the distance from the meniscus rises, the local solidification time in the mushy zone increases linearly, and the cooling rate of this zone decreases rapidly. Overall and local solidification rate decreases throughout the billet length, but the local solidification rate experiences a sudden increase at the beginning of the mushy core. The behavior of brittle zone width is similar to that of the mushy zone, but the slope of its decrease is much greater.

1. Introduction

It is well known that some quality criteria of continuously cast ingots depend on the characteristics of the mushy zone during solidification. The degree of microsegregation and macrosegregation, the ratio of equiaxed to columnar grains, and the hot tearing tendency are examples of these criteria. For instance, in microsegregation modeling, it is necessary to consider specific regions of the mushy zone. Also, the cooling rate of the mushy zone is essential, in studying the microsegregation phenomenon [1-2]. It has been proven that the characteristics of the mushy zone affect the macrosegregation behavior of steels in continuous casting, and this issue has been considered in macrosegregation modeling [3]. It has been reported that the dimensions of the melt core (and consequently the dimensions of the mushy zone) affect the size of the secondary dendritic arms [4], which in turn affects the interdendritic melt enriched with alloying elements. The casting temperature

* *Corresponding Author*
Email: mostafa_alizadeh56@yahoo.com
Address: Department of Materials Science and Engineering, School of Engineering, Meybod University, Meybod, Yazd, Iran
1. Associate Professor

DOI: http://10.22034/IJISSI.2025.2048426.1313
Published by ISSI (Iron & Steel Society of Iran)

affects macrosegregation [5]. On the other hand, it is well-established that the casting temperature also significantly influences the characteristics of the mushy zone. Therefore, the characteristics of the mushy zone directly influence macrosegregation behavior. The casting speed (which affects the characteristics of the mushy zone) affects the equiaxed grains ratio in the mushy zone, such that as the casting speed increases, the ratio of equiaxed grains decreases [6]. The temperature gradient in the mushy zone and the growth rate of dendrites change along the length of the strand [6]. It has been stated that the cooling rate in the mold and casting speed affect the thickness of the equiaxed region formed in the mushy zone [7]. According to a comprehensive review, in the final stages of solidification in the mushy zone, a thin film of melt is formed, which is called the weak or brittle zone, where hot tear defects can create in this zone [8]. It has been proven that the thickness of the brittle zone plays a significant role in the formation of hot tears, and the tendency to form hot tears increases with the increase in the thickness of this zone [9]. It has been emphasized that during continuous casting of steels, internal and surface cracks are formed in the brittle zone under thermal and mechanical deformations, and to prevent these defects, it is essential to have a correct understanding of the mechanical behavior of the ductile zone. In this regard, it is required to evaluate characteristic temperatures in the mushy zone [10].

Various researchers have pointed out the importance of the mushy zone in continuous casting simulation. Still, there is no consistent research on the required mathematical models, method of definition and determining the characteristics of the mushy zone by simulation of continuous casting. Especially since some quality control criteria in continuous casting products are related to the characteristics of the mushy zone. Therefore, the primary objective of this research is to propose straightforward mathematical models and a simplified simulation process to define the mushy zone and determine its characteristics during the continuous casting of steel.

2. Simulation and Research Method

2.1. Governing Conditions During Continuous Casting

In this research, a curved billet production machine was considered that is capable of producing steel billets with cross-sectional dimensions of 150 mm×150 mm. The schematic of the billet being made by this machine is shown in Fig. 1. In this drawing, the billet curve is omitted, but the various cooling zones are shown schematically. As can be seen, billet cooling occurs in the mold zone (primary cooling) and the sub-mold zone (secondary cooling). The secondary cooling zone mainly includes forced convection cooling (by water spray), natural convection, radiation, and thermal conduction through the contact of the support rollers [11-13].

It can be seen from Fig. 1. that water spray cooling consists of 5 zones that differ in length and cooling water flow rate. In the present study, the length of each cooling zone and the corresponding cooling water flow rate collectively define the cooling pattern, the detailed parameters of which are provided in Table 1. The steel's chemical composition is presented in Table 2. and the operational conditions of the continuous casting process are summarized in Table 3.

2.2. Governing Equations and Simulation Assumptions

In order to study the mushy zone in the continuous casting process, solidification simulation was used. In this regard, the following assumptions were considered:

1. Heat transfer along the length of the billet (z direction in Fig. 1.) is negligible compared to the cross-section of the billet (x and y directions), so the cross-section of the billet can be chosen as the two-dimensional computational domain.
2. In the cross-section of the billet, heat transfer occurs symmetrically, so only one-quarter of the cross-section can be selected as the calculation domain.
3. The billet curvature is ignored, and therefore, the cooling intensity of the sprays is considered independent of the convexity or concavity of the billet surface.
4. Forced convection is the most effective heat transfer mechanism in the secondary cooling zone [14]. After that, the radiation contributes significantly to the heat transfer (because it covers a considerable length of the secondary zone). The effects of roller contact and natural convection on the cooling of the secondary zone are neglected.

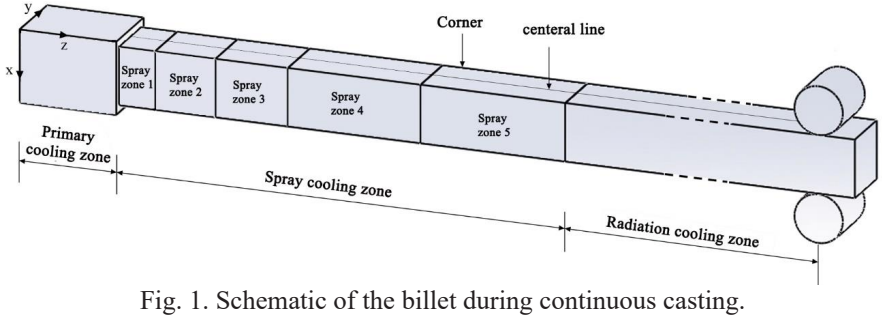

Fig. 1. Schematic of the billet during continuous casting.

Table 1. The cooling pattern during continuous casting.

Cooling zone type		Length of any zone (m)	Water flow rate in any zone (L/min)
Mold		0.9	2000
Spray	Zone1	0.4	37.2
	Zone2	0.6	22
	Zone3	1	28.9
	Zone4	2.5	29
	Zone5	2.8	31.3
Radiation		29	-----

Table 2. Chemical composition of steel.

Wt%C	Wt%Mn	Wt%Si	Wt%Cr	Wt%S	Wt%P	Others
0.66	0.78	0.24	0.56	0.003	0.0015	Iron

Table 3. Continuous casting operating parameters.

Casting speed (m/min)	Pouring temperature (°C)	water temperature of sprays (°C)	water temperature of mold (°C)
1.5	1511	25	25

According to assumptions 1 and 2, the following two-dimensional unsteady heat transfer equation was used to simulate solidification. This equation was discretized using the finite difference numerical method (FDM), and the corresponding equations were coded and solved.

$$\rho(T)C'(T)\frac{\partial T}{\partial t} = k(T)\left(\frac{\partial^2 T}{\partial x^2} + \frac{\partial^2 T}{\partial y^2}\right) \quad \text{Eq.(1)}$$

Eq.(2)

$$C'(T) = \begin{cases} C_l(T) & T_{liq} < T \\ C(T) - \Delta H_m\left(\frac{\partial f_s}{\partial T}\right) & T_{sol} \le T \le T_{liq} \\ C_s(T) & T < T_{sol} \end{cases}$$

To convert the energy equation to the solidification equation, it is necessary to include the phase change phenomenon in the energy equation. For this purpose, the effective heat capacity (Eq. 2) was used, which has also been used by some other researchers [12, 15-16]. In the equations above, t is time (s), T is temperature (K), f_s is the solid fraction, and ΔH_m is the latent heat of fusion (J/kg). The thermophysical properties C(T), k(T), and ρ(T) are the heat capacity (J/kg·K), thermal conductivity (W/m·K), and density (kg/m³), respectively. These properties are given as functions of temperature in Table 4.

In the equations above, t is time (s), T is temperature (K), f_s is the solid fraction, and ΔH_m is the latent heat of fusion (J/kg). The thermophysical properties C(T), k(T), and ρ(T) are the heat capacity (J/kg·K), thermal conductivity (W/m·K), and density (kg/m³), respectively. These properties are given as functions of temperature in Table 4.

To calculate the values of thermo-physical properties in the mushy zone, Eq. 3 was used. In this equation, ϕ represents each of the thermo-physical properties, and the subscripts s and l are for the solid and liquid phases, respectively.

$$\emptyset(T) = [\emptyset_s(T) - \emptyset_l(T)].f_s + \emptyset_l(T) \quad \text{Eq.(3)}$$

To calculate the solid fraction (f_s) in the above equations, the equilibrium lever law (Eq. 4) was used. In this equation, k_0 represents the equilibrium partition coefficient, T_l represents the liquidus temperature, and T_f represents the melting temperature of the base metal (iron).

$$f_s = \left(\frac{1}{1-k_0}\right).\left(\frac{T_l - T}{T_f - T}\right) \quad \text{Eq.(4)}$$

Table 4. Thermo-physical properties of steel.

Thermo-physical parameter type	Thermo-physical parameter value
Conductivity of liquid steel (W/m/k)	39
Conductivity of solid steel (W/m/k)	$21.6+8.35\times10^{-3}T$
Density of liquid steel (kg/m^3)	7965.98-0.619T
Density of solid steel (kg/m^3)	8105.91-0.5091T
Heat capacity of liquid steel (J/kg/k)	824.6157
Heat capacity of solid steel (J/kg/k)	$429.849+0.1498\times10^{-3}T$

Boundary conditions:

Fig. 2. shows the computational domain and boundary conditions. As shown, one-quarter of the billet's cross-section is considered the computational domain.

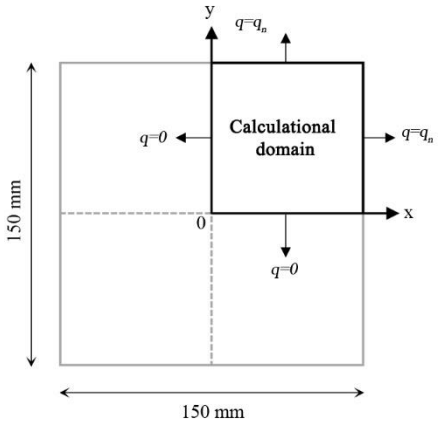

Fig. 2. Billet cross-section and calculation domain (which is equal to one-quarter of the cross-section) along with boundary conditions.

At the beginning of solidification, t=0, and the initial temperature at the highest height of the billet (z=0) is equal to the pouring temperature ($T_{pouring}$):

Eq.(5)

$$T = T_{pouring} \qquad at \quad z = 0 \ and \ \ t = 0$$

The boundary condition in the primary cooling zone (mold), spray zone and radiation zone is considered to be heat flux (q_n) and therefore the heat transfer boundary condition equation is calculated with Eq. 6. In this equation, the term of n represents the direction perpendicular to the surface and the term of q_n (in W/m^2) represents the local heat flux density which is zero at the symmetry boundaries (center line in Fig. 2.) and is calculated at the outer boundaries by Eq.6.

Eq.(6)

$$\begin{cases} -k(T)\dfrac{\partial q}{\partial n} = q_n & \\ \dfrac{\partial q}{\partial n} = \dfrac{\partial q}{\partial x} & (0 \le y \le y_{surface}) \\ \dfrac{\partial q}{\partial n} = \dfrac{\partial q}{\partial y} & (0 \le x \le x_{surface}) \end{cases}$$

In this study, the heat flux along the mold was calculated using Eqs. (7) (9). which has also been used by some other researchers [11, 17-19]. In these equations, q_n is calculated along the mold length.

$$q_n = 2680000 - b\sqrt{z/V_c} \qquad \text{Eq.(7)}$$

$$b = 1.5(2680000 - \overline{q})/\sqrt{L_m/V_c} \qquad \text{Eq.(8)}$$

$$\overline{q} = \frac{\rho_w C_w Q_m \Delta T_w}{S} \qquad \text{Eq.(9)}$$

The term b in Eq. (7) is a function of the water flow rate, the temperature difference between the inlet and outlet water, the mold length, and the effective mold surface area, and is calculated using Eqs. (8) and (9). In the above equations, Z (in m) is the distance from the meniscus in the mold, L_m (in m) is the effective mold length, and V_c (in m/s) is the casting speed. In Eq.9. $\overline{q}$ (in W/m^2) is the average heat flux in the mold, ρ_w (in kg/m^3) is the density of water, C_w (in j/kg/k) is the specific heat of the mold water, Q_m (in l/min) is the mold water flow rate, and ΔT_w is the temperature difference between the inlet and outlet water of the mold.

The local heat flux density of the sprays in the secondary cooling zone is calculated by Eq.10. In this equation, T_s is the billet surface temperature, T_{spray} is the spray water temperature (in ^{o}C), and h_i (in W/m^2/K) is the spray heat transfer coefficient. The subscript i indicates the number of spray cooling zones with different length

and different water flow rates, which in the casting machine considered in this study, i varies from 1 to 5. In this study, Eq.11 was used to calculate the heat transfer coefficient of sprays, which has also been used by other researchers [20-21].

$$q_n = h_i\left(T_s - T_{spray}\right) \quad \text{Eq.(10)}$$

$$h_i = \frac{1570.Q_w^{0.55}.(1-0.0075T_{spray})}{\alpha} \quad \text{Eq.(11)}$$

The term Q_w (in l/m²·s) is the water flow rate in the secondary cooling zone, and α is a correction parameter that depends on the casting machine. In the present study, α is taken to be equal to 4 [21–22]. The radiant heat flux is calculated by Eq. 12, where T_s and T_{amb} are the billet surface temperature and ambient temperature (in °C), respectively. The term ε represents the emissivity of the steel surface and is taken as 0.8 in this study, while σ denotes the Stefan–Boltzmann constant (5.67×10^{-8} W/m²·K⁴).

$$q_n = \sigma\varepsilon[(T_s + 273)^4 - (T_{amb} + 273)^4] \quad \text{Eq.(12)}$$

In this study, analytical microsegregation models were used to calculate characteristic temperatures in the mushy zone. For this purpose, the Klyne-Kutz microsegregation model [23] was used, which has also been used previously by Seol et al. [24].

$$T = 1536 - [\sum f'(C_i)].[1 - f_s(1 - 2\Omega k)]^{\frac{k-1}{1-2\Omega k}} \quad \text{Eq.(13)}$$

$$\sum f'(C_i) = 67.5(wt\%C) + 9.741(wt\%Si) + 3.292(wt\%Mn) + 82.18(wt\%P) + 155.8(wt\%S) \quad \text{Eq.(14)}$$

$$\Omega = \alpha\left(1 - exp(-1/\alpha)\right) - \frac{1}{2}exp(-1/2\alpha) \quad \text{Eq.(15)}$$

$$\alpha = 33.7\ CR^{-0.244} \quad \text{Eq.(16)}$$

In the above equations, C_i is the chemical composition of the steel and CR is the cooling rate, α and Ω are parameters that express the degree of back-diffusion of alloying elements, and k is equal to 0.265 and is the average equilibrium partition coefficient of carbon in the austenite and delta ferrite phases.

3. Results and Discussion

3.1. Validation of Simulation

To validate the simulation in this study, the simulated temperature was compared with the temperature measured by the thermography camera. This comparison is shown in Fig. 3. Due to limited access to the entire length of the billet, temperature measurements were performed only in the fifth spray zone and the radiation zone. As Fig. 3. shows, there is good agreement between the measured and simulated data, indicating that the model used in this study is valid. However, the measured temperatures are slightly lower than the simulated values, which is probably due to the presence of an oxide layer on the billet surface.

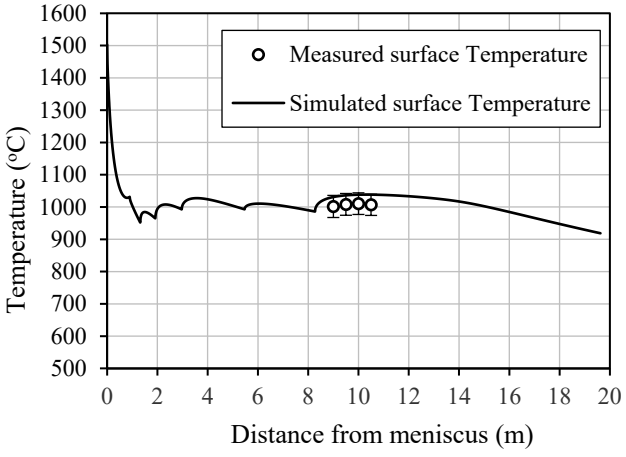

Fig. 3. Billet surface temperature changes along the length of the billet for the conditions mentioned in Tables 1, 2 and 3.

3.2. Definition and Determination of the Mushy Zone in Continuous Casting

In simple terms, the region enclosed between the liquidus (corresponding to the solid fraction f_s=0) and solidus (corresponding to the solid fraction f_s=1) temperatures is called the mushy zone, which contains a mixture of molten and solid phases. In addition to the liquidus (T_{liq}) and solidus (T_{sol}) temperatures, three other essential temperatures are also defined in the mushy zone, which are used to determine the mechanical properties of the mushy zone. These temperatures are: the zero strength temperature (ZST), liquid infiltration temperature (LIT), and zero ductility temperature (ZDT). Therefore, in determining the plastic zone in the continuous casting process, it is necessary to decide on these temperatures

as well. The ZST is the temperature above which there is no significant connection between the dendrites, and the strength of the mushy zone is zero. The LIT is the temperature at which the dendrites are connected and form a continuous network that makes it difficult for the liquid phase to penetrate between the dendritic arms, and therefore, at temperatures below that, the melt does not feed the network between the dendrites. The ZDT is the temperature above which the mushy zone lacks ductility. According to Won et al. [25], the ZST, LIT, and ZDT correspond to solid fractions of 0.75, 0.9, and 0.99, respectively. To determine the mushy zone in continuous casting, it is first necessary to calculate the values of the characteristic temperatures using microsegregation equations (Eqs. 13, 16), and then calculate the distance from the billet surface to the location corresponding to each of the above temperatures at each solidification time. To convert the solidification time to the distance from the meniscus and determine the mushy zone along the length of the billet, Eq. 17 is used. In this equation, z (in m) is the distance from the meniscus in the mold, V_c (in m/s) is the casting speed, and t (in s) is the solidification time.

$$z = \frac{t \times V_c}{60} \qquad \text{Eq.(17)}$$

Under the conditions specified in Tables 1, 2 and 3. with a cooling rate of 0.17 °C/s, the values for T_{liq}, ZST, LIT, and ZDT will be 1486 °C, 1436.7 °C, 1412.37 °C and 1391 °C, respectively.

Fig. 4. shows the distance from the billet surface to the location of each characteristic temperature along the length of the billet, and is called the solidification diagram. The data in Fig. 4. were extracted along the x- or y-axis in Fig. 2.

Since ZDT is approximately equal to the solidus temperature (because ZDT corresponds to a solid fraction of f_s=0.99, which is very close to f_s=1), the graph of ZDT can be considered as a fully solidified shell thickness along the length of the billet. Logically, the solidification of the billet is complete when the thickness of the fully solidified shell reaches the middle of the billet (i.e., 0.075 m from the billet surface). Therefore, as Fig. 4. shows, the solidification of this billet is completed at a length of 12.94 m.

The liquid core (metallurgical length) exists until the liquidus temperature reaches the center of the billet. Therefore, according to Fig. 4. the depth of the liquid core in the billet is 5.57 m. Fig. 5. shows the solid fraction contour in the longitudinal section of the billet for the conditions mentioned in Tables 1, 2 and 3. As shown in this figure, there is a liquid core up to a distance of 5.57 m from the meniscus, and after that, there is a mushy core up to a depth of 12.94 m.

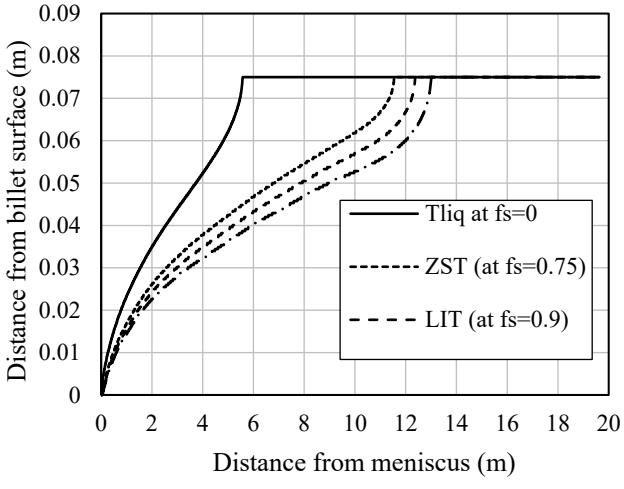

Fig. 4. Distance from the billet surface to the locations corresponding to the T_{liq}, ZST, LIT, and ZDT isotherms along the billet length under the conditions specified in Tables 1, 2 and 3.

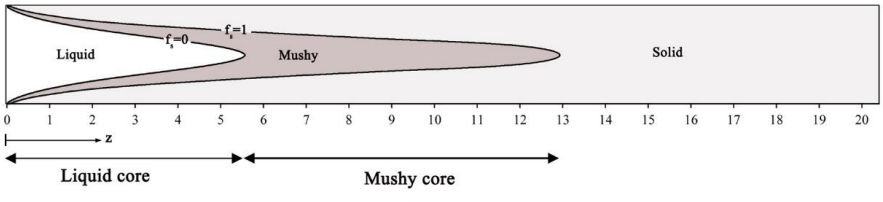

Fig. 5. Solid fraction contour in the longitudinal section of the billet for the conditions mentioned in Tables 1, 2 and 3.

3.3. Width and Total Area of Mushy Zone

The width of the mushy zone (L_m) is an essential characteristic of the mushy zone. It is obtained using the solidification diagram (Fig. 4) and Eq.18. In this equation, $d_{fs=1}$ and $d_{fs=0}$ are the distances from the billet surface to the location corresponding to the solidus temperature and liquidus temperature, respectively, and are obtained using Fig. 4.

Eq.(18)

$$L_m = \begin{cases} d_{f_s=0} - d_{f_s=1} & z \le mushy\ core\ beginning \\ d_{f_s=0} - 2d_{f_s=1} & z > mushy\ core\ beginning \end{cases}$$

Fig. 6. shows the variation of the width of the mushy zone along the length of the billet. As this figure shows, the width of the mushy zone increases continuously from the meniscus to a depth of 5.57 m (the depth of the liquid core) and reaches a value of 0.036 m. At the end of the liquid core (i.e., the beginning of the mushy core), the width of the mushy zone increases abruptly—doubling in this case. This occurs because the mushy zones formed on both sides of the billet meet and merge at the center. Subsequently, the width decreases until it reaches zero at a depth of 12.94 m. The peak of the curve in Fig. 6. indicates the boundary between the liquid core and the mushy core. The area under the curve represents the total area of the mushy zone in the billet. Both the total area of the mushy zone and the depth of the mushy core can be considered as criteria for the billet's susceptibility to solidification defects. According to Fig. 6. for the conditions specified in Tables 1, 2, and 3. the depth of the mushy core and the total area of the mushy zone are 7.36 m and 0.434 m², respectively.

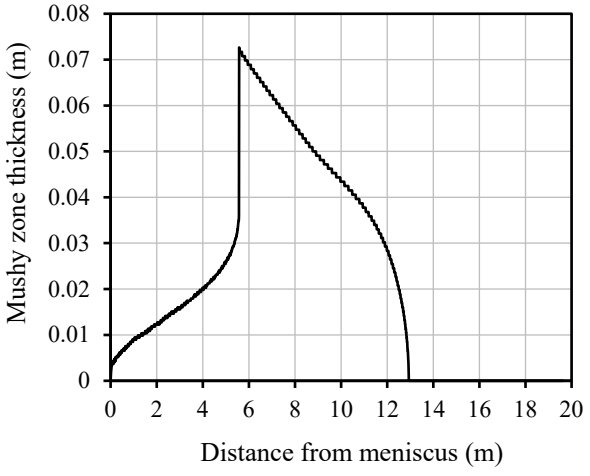

Fig. 6. The width of the mushy zone along the billet for the conditions mentioned in Tables 1, 2 and 3.

3.4. Temperature Changes in the Centerline of the Mushy Core

Usually, in the investigation of phenomena associated with solidification (such as hot tearing), it is essential to study the temperature profile of the mushy zone. Fig. 7. shows the temperature profile at the centerline of the billet in the mushy core (from z=5.57m to z=12.94m). As Fig. 7. shows, the upper limit of the centerline temperature in the mushy core is the liquidus temperature, and the lower limit is the solidus temperature. At the centerline of the billet, the temperature at the beginning of the mushy core (z=5.57m in Fig. 5.) is equal to the liquidus temperature. Upon entering the mushy core, the billet centerline temperature initially decreases slowly, but as it approaches the end of the core (solidus temperature), the centerline temperature decreases more rapidly. The temperature gradient in the core centerline (dT/dz) is also shown in Fig. 7. As can be seen, at the end of the mushy core (z = 12.94 m in Fig. 5.), the temperature gradient is about 50 °C/m, whereas at the beginning of the core, this value is nearly zero.

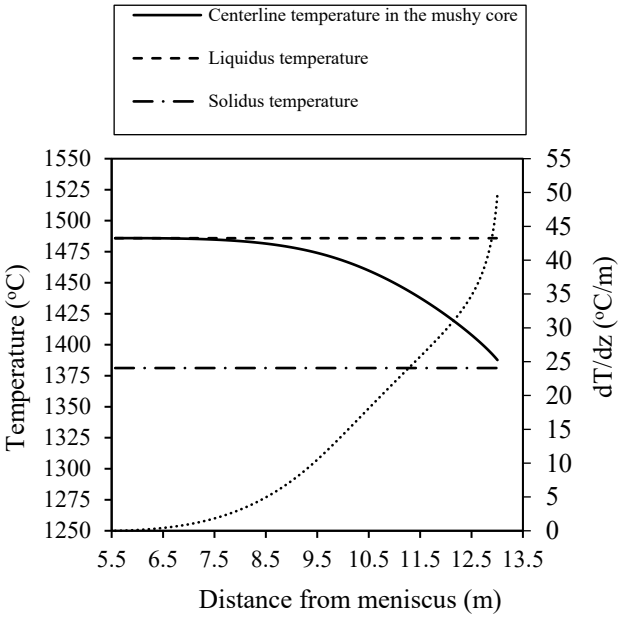

Fig. 7. Temperature profile and temperature gradient at the centerline of the mushy core for the conditions mentioned in Tables 1, 2 and 3.

3.5. Investigation of local solidification time and local cooling rate in the mushy zone

In predicting the microstructure, for example, the secondary dendrite arm spacing, the local solidification rate (CR in °C/s) is essential [2]. The following equation is used to calculate the local solidification rate:

$$CR = \frac{T_{liq} - T_{sol}}{t_f} \quad \text{Eq.(19)}$$

In this equation, t_f (in s) is the local solidification time and is defined as the time it takes for the liquidus temperature to reach the solidus temperature. Fig. 8. shows how to calculate the local solidification time for two arbitrary locations (for example, z = 4m and z = 10m). In fact, Fig. 8. shows the distance from the billet surface to the location corresponding to T_{liq} and T_{sol} as a function of solidification time. To calculate t_f at each location along the length of the billet, first, the desired area is converted to solidification time by Eq.18 and then the local solidification time is calculated according to Fig. 8. Based on Eq.18, the time corresponding to 4 m and 10 m is equal to 152.8 and 382.16 seconds, respectively.

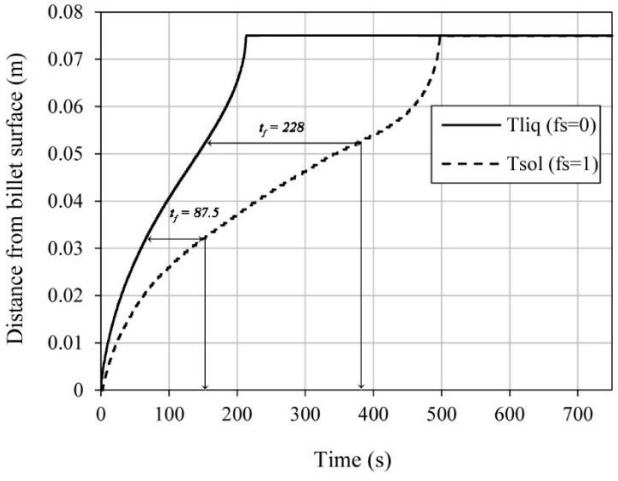

Fig. 8. Distance from the billet surface to the isothermal lines T_{liq} and T_{sol} along the billet and method for calculating the local solidification time.

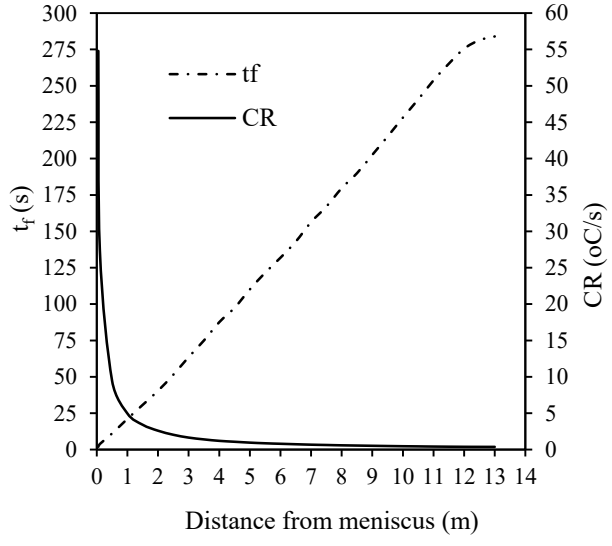

Fig. 9. The local solidification time and local cooling rate along the billet length.

Fig. 9. shows the variations of the local solidification time and the local cooling rate along the length of the billet. As can be seen, the local solidification time increases along the length of the billet, reaching 284 s at the end of solidification (z = 12.94 m). Fig. 9. also shows the local cooling rate in the mushy zone. It is observed that this quantity decreases along the length of the billet, so that the highest local cooling rate is in the mold zone, which reaches about 55 °C/s, and at the end of freezing, it has its lowest value, reaching about 0.36 °C/s.

3.6. Investigation of Overall and Local Solidification Rate

Determining the solidification rate is an essential step in predicting the microstructure and grain size. By definition, the overall solidification rate is the thickness of the fully solidified shell divided by the overall solidification time. In the continuous casting process, this quantity can be calculated along the length of the billet. To do this, at any desired length of the billet, the thickness of the fully solidified shell (the line corresponding to f_s = 1 in Fig. 8.) is divided by the solidification time. Fig. 10. shows the overall solidification rate along the length of the billet. It is observed that the overall solidification rate first increases in the mold region and then decreases continuously until the end of solidification. For the conditions mentioned in Tables 1, 2 and 3. the highest overall solidification rate is 0.00049 m/s, which decreases to 0.00015 m/s at the end of solidification (z = 12.94 m).

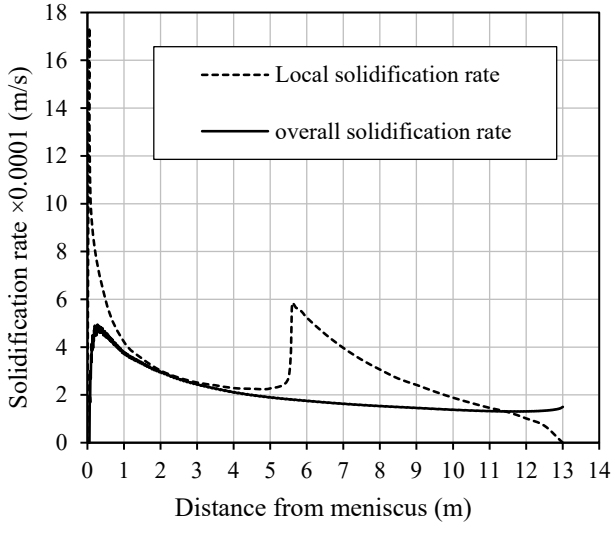

Fig. 10. the overall and local solidification rate along the billet length.

To calculate the local solidification rate, the thickness of the mushy region (in Fig. 6.) is divided by the local solidification time (in Fig. 9). Fig. 10. shows the variations of the local solidification rate. As can be seen, the local solidification rate reaches a maximum value with a fast slope. This behavior indicates that the mushy zone is

formed very quickly in the mold. The local solidification rate decreases continuously until the beginning of the mushy core. At this point, as the thickness of the mushy zone doubles, the local solidification rate also doubles. It then decreases rapidly until the end of the mushy core, reaching zero.

3.7. Investigation of Brittle Region in the Mushy Zone

Determining the brittle temperature range (ΔT_B) is an essential issue for investigating the tendency of internal cracks to form during solidification, and many researchers have pointed out its importance [9, 24]. Most researchers accept that within this temperature range, a liquid film rich in alloying elements exists due to microsegregation, leading to reduced ductility in this region. In definition, the temperature range between LIT and ZDT is known as the brittle temperature range [10] and is calculated as follows:

$$\Delta T_B = LIT - ZDT \qquad \text{Eq.(20)}$$

Previous research has shown that the width of the brittle zone (ΔS_B) has a significant effect on the formation of hot tears [9] and is calculated as follows:

Eq.(21)

$$\Delta S_B = \begin{cases} d_{LIT} - d_{ZDT} & z \le mushy\ core\ beginning \\ d_{LIT} - 2d_{ZDT} & z > mushy\ core\ beginning \end{cases}$$

Fig. 11. shows the variation of the width of the brittle zone along the length of the billet. It can be seen that the width of the brittle zone increases slowly from the beginning of solidification (meniscus) to a certain length of the billet (z=12m) and reaches 5 mm. Then it increases suddenly up to a distance of 12.4 m to 11 mm. At this point, the brittle zone reaches the center of the billet, and therefore it doubles to about 22 mm. Finally, it decreases rapidly and reaches zero. The distance from the mushy core over which the width of the brittle zone decreases from its maximum value to zero is defined as the brittle core, measuring 0.6 m. The area under the graph in Fig. 11. represents the total area of the brittle zone and is equal to 0.043 m^2.

4. Conclusions

In this study, continuous casting simulation was used. The characteristics of the mushy zone of 1.2007 medium carbon steel billet with a cross-section dimension of 150×150 mm^2 were investigated and the following results were obtained in summary:

- The width of the mushy zone first increases and then decreases along the length of the billet. The distance over which the width of the mushy zone decreases is referred to as the mushy core and has a relatively large depth. The beginning of the mushy core is located at the liquidus temperature and its end is located at the solidus temperature.
- The depth of the mushy core (for the conditions mentioned in this study) is about 7.43 m, which is greater compared to the depth of the liquid core (5.57 m). This result shows that the continuous casting process is susceptible to defects caused by the mushy zone.
- The slope of the temperature profile in the mushy core increases rapidly.
- By analyzing the solidification diagram in the mushy zone, the local solidification time and consequently the local cooling rate can be obtained. The local solidification time increases linearly along the length of the billet, and the local cooling rate decreases almost rapidly along the length of the ingot.
- The overall solidification rate decreases continuously along the billet length while the local solidification rate experiences a sudden increase during reduction along the billet length. This increase happens at the beginning of the mushy core.
- Similar to the mushy zone width, the brittle zone width initially increases and then decreases to zero. However, the rate of reduction in the brittle zone

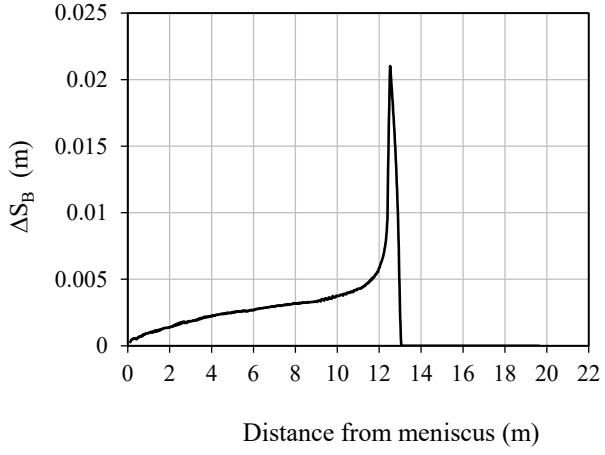

Fig. 11. the width of the brittle zone along the billet zone.

width is greater than that of the mushy zone width, and the brittle core is shorter than the mushy core along the billet centerline.
- In the present research, the area under the mushy zone width diagram was defined as the total mushy zone area.

Acknowledgment

The author of this article would like to thank the officials of the Research and Development Unit of Iran Alloy Steel Company for their cooperation in collecting the data required for this article.

Conflict of Interest

The author states that there is no conflict of interest to declare

References

[1] Wang W, Zhu M, Cai Z, Luo S, Ji C, Micro-segregation behavior of solute elements in the mushy zone of continuous casting wide-thick slab. Steel Res Int. 2012; 83: 1–11.
[2] Won Y.M, Thomas B.G, Simple model of microsegregation during solidification of steels, Metall Mater Trans A. 2001; 32: 1755–67.
[3] Pequet C.H, Gremaud M, Rappaz M, Modeling of microporosity, macroporosity, and pipe-shrinkage formation during the solidification of alloys using a mushy-zone refinement method: applications to aluminum alloys, Metall Mater Trans A. 2002; 33: 2095–106.
[4] Gao Y, Bao Y, Wang M, Zhang M, On the macrosegregation of continuous casting of high carbon steel billet with strand reduction process, Metals. 2024; 14: 157.
[5] Quinelato F.P, Garcao W.J.L, Paradela K.G, Sales R.C, Baptista L.A.S, Ferreira A.F, An experimental investigation of continuous casting process: effect of pouring temperatures on the macrosegregation and macrostructure in steel slab. Mater Res. 2020; 23: e20200023.
[6] Kim J.C, Kim J.J, Choi J.Y, Choi J.H, Kim S.K, Control of columnar-to-equiaxed transition in continuous casting of 16%Cr stainless steel. La Metall Ital. 2009: 43–8.
[7] Yang X.G, Xu Q.T, Wu C.L, Chen Y.S, Experimental study of the continuous casting slab solidification microstructure by the dendrite etching method, Mater Sci Eng. 2017; 283: 012017.
[8] Eskin D.G, Suyitno, Katgerman L, Mechanical properties in the semi-solid state and hot tearing of aluminium alloys, Prog Mater Sci. 2004; 49: 629–711.
[9] Alizadeh M. Study on hot tearing tendency during continuous casting of steel by overall hot tearing susceptibility (OHTS). Int J Cast Met Res. 2015; 28: 20–7.
[10] Kim K.H, Yeo T.J, Oh K.H, Lee D.N, Effect of carbon and sulfur in continuously cast strand on longitudinal surface cracks. ISIJ Int. 1996; 36: 284–9.
[11] Mosayebidorcheh S, Gorji-Bandpy M, Solidification and thermal performance analysis of the low carbon steel during the continuous casting process, J Adv Mater Process. 2017; 5: 3–11.
[12] Meng Y.A, Thomas B.G, Heat-transfer and solidification model of continuous slab casting: CON1D, Metall Mater Trans B. 2003; 34: 685–705.
[13] Petrus B, Zheng K, Zhou X, Thomas B.G, Bentsman J, Real-time, model-based spray-cooling control system for steel continuous casting, Metall Mater Trans B. 2011; 42: 87–103.
[14] Sadat M, Honarvar Gheysari A, Sadat S, The effects of casting speed on steel continuous casting process, Heat Mass Transf. 2011; 47: 1601–9.
[15] Ma J, Xie Z, Jia G, Applying of real-time heat transfer and solidification model on the dynamic control system of billet continuous casting, ISIJ Int. 2008; 48: 1722–7.
[16] Yu Y, Luo X, Zhang H.Y, Zhang Q, Dynamic optimization method of secondary cooling water quantity in continuous casting based on three-dimensional transient nonlinear convective heat transfer equation, Appl Therm Eng. 2019; 160: 113988.
[17] Liu Q, Wang L, Zhang L, Cao L, Ding X, Liang M, Qi Y, Mathematical model of heat transfer for bloom continuous casting, J Univ Sci Technol Beijing. 2008; 15: 17–23.
[18] Zeng J, Chen W, Wang Q, Wang G, Improving inner quality in continuous casting rectangular billets: comparison between mechanical soft reduction and final electromagnetic stirring. Trans Indian Inst Met. 2016; 69: 1623–32.
[19] Yang B, Deng A, Li Y, Xu X, Wang E, Numerical simulation of flow and solidification in continuous casting process with mold electromagnetic stirring. J Iron Steel Res Int. 2019; 26: 219–29.
[20] Pourfathi A, The effect of slab thickness on the solidification of low carbon steel in continuous casting process: a simulation case study, Int J ISSI. 2022; 19: 67–80.
[21] Hardin R.A, Kailiu, Kapoor A, Beckermann C, A transient simulation and dynamic spray cooling control model for continuous steel casting. Metall Mater Trans B. 2003; 34: 297–306.
[22] Sismanis P, Evaluation of solidification times for medium and high carbon steels based upon heat transfer and solidification phenomena in the continuous casting of blooms. In: Heat Transfer Studies and Applications. 2015; 12: 315–39.
[23] Clyne T.W, Kurz W, Solute redistribution during solidification with rapid solid state diffusion, Metall Mater Trans A. 1981; 12: 965–71.
[24] Seol D.J, Won Y.M, Oh K.H, Shin Y.C, Yimi C.H, Mechanical behavior of carbon steels in the temperature range of mushy zone, ISIJ Int. 2000; 40: 356–63.
[25] Won Y.M, Kim K, Yeo T.J, Oh K.H, Effect of cooling rate on ZST, LIT and ZDT of carbon steels near melting point. ISIJ Int. 1998; 38: 1093–9.